Journal of High Energy Astrophysics 42 (2024) 209–216

Contents lists available at ScienceDirect

Journal of High Energy Astrophysics

journal homepage: www.elsevier.com/locate/jheap

Probing the universe's expansion dynamics: The linear correction scenario perspective on dark energy

Yerlan Myrzakulov [a,b,*], M. Koussour [c], M. Karimov [d,e], J. Rayimbaev [f,g,h]

[a] Department of General & Theoretical Physics, L.N. Gumilyov Eurasian National University, Astana, 010008, Kazakhstan
[b] Ratbay Myrzakulov Eurasian International Center for Theoretical Physics, Astana, 010009, Kazakhstan
[c] Department of Physics, University of Hassan II Casablanca, Morocco
[d] Institute of Fundamental and Applied Research, National Research University TIIAME, Kori Niyoziy 39, Tashkent 100000, Uzbekistan
[e] Faculty of Mathematics, Namangan State University, Bobursho str. 161, Namangan 160107, Uzbekistan
[f] New Uzbekistan University, Mustaqillik Ave. 54, Tashkent 100007, Uzbekistan
[g] University of Tashkent for Applied Sciences, Gavhar Str. 1, Tashkent 100149, Uzbekistan
[h] National University of Uzbekistan, Tashkent 100174, Uzbekistan

ARTICLE INFO

Keywords:
Dark energy
Hubble parameter
KMMS models
Observational constraints

ABSTRACT

In this study, we investigate the cosmological evolution of the universe, focusing on the KMMS models in a model-independent approach, particularly the scenario involving linear correction, given by $E^2(z) = A(z) + \beta(1+\gamma B(z))$, where $A(z) = \Omega_{m0}(1+z)^3$ and $B(z) = z$. By analyzing recent Cosmic Chronometers (CC) and the $Pantheon^+$ samples, we determine the best-fit values of model parameters using a Markov chain Monte Carlo analysis. Our models exhibit unique dynamics, transitioning from super-exponential to exponential expansion, with a significant shift at redshift $z_t = 0.83^{+0.11}_{-0.10}$ and present deceleration parameter $q_0 = -0.69^{+0.17}_{-0.17}$. The jerk parameter exceeds 1, indicating a faster change in acceleration than predicted by ΛCDM. The energy density parameter is consistent with Planck observations, and the dark sector evolution follows the expected thermal history. The EoS parameter approaches $\omega_{de} = -1$ over time, with a current value of $\omega_{de0} = -1.06 \pm 0.12$, aligning with the phantom phase. Our model presents a new dark energy alternative, emphasizing the importance of considering models like KMMS in understanding cosmic evolution.

Contents

* Corresponding author at: Department of General & Theoretical Physics, L.N. Gumilyov Eurasian National University, Astana, 010008, Kazakhstan.
E-mail addresses: ymyrzakulov@gmail.com (Y. Myrzakulov), pr.mouhssine@gmail.com (M. Koussour), karimovmuzaffar050@gmail.com (M. Karimov), javlon@astrin.uz (J. Rayimbaev).

https://doi.org/10.1016/j.jheap.2024.05.006
Received 9 April 2024; Received in revised form 10 May 2024; Accepted 14 May 2024
Available online 16 May 2024

1. Introduction

General Relativity (GR) stands as a foundational theory in the study of gravitational interactions, forming the bedrock upon which our understanding of cosmic dynamics is built. Within this framework, the ΛCDM (Λ Cold Dark Matter) model emerges as a consistent and successful cosmological model, aligning with a wide array of observational data and theoretical predictions. However, despite the remarkable success of GR and the ΛCDM model, several challenges have emerged, both of theoretical and observational nature. The theoretical challenges include the cosmological constant problem, which revolves around the perplexing discrepancy between the predicted and observed value of the cosmological constant, leading to questions about the nature of dark energy (DE) (Weinberg, 1989). Another theoretical issue is the coincidence problem, which questions the apparent alignment of the energy densities of dark matter and DE in the current epoch, despite their vastly different behaviors over cosmic history (Steinhardt et al., 1999). In addition, the non-renormalizability of GR poses a fundamental challenge from a theoretical perspective, hinting at potential limitations of the theory in extreme conditions such as those found in the early universe or near black holes. On the observational front, challenges such as the Hubble tension and the σ_8 tension have garnered attention. The Hubble tension refers to the discrepancy between the measurements of the present-day expansion rate of the universe derived from local measurements (such as those from the Hubble Space Telescope) and those inferred from the cosmic microwave background (CMB) observations within the framework of the ΛCDM model. Similarly, the σ_8 tension concerns the mismatch between the amplitude of matter density fluctuations inferred from the CMB and large-scale structure observations (Addazi et al., 2022; Abdalla et al., 2022; Martin, 2012; Freedman, 2017; Lusso et al., 2019; Lin et al., 2020; Perivolaropoulos and Skara, 2022). These challenges, both theoretical and observational, underscore the need for continued exploration and refinement of our cosmological models, as well as the potential for new physics beyond the current paradigms. Consequently, numerous modified gravity theories have been developed (Buchdahl, 1970; Kleinert and Schmidt, 2002; Odintsov and Oikonomou, 2017; Capozziello et al., 2018, 2011; Liu and Reboucas, 2012; Jimenez et al., 2018, 2020), and several models beyond the ΛCDM framework have been proposed (Ratra and Peebles, 1998; Sami and Toporensky, 2004; Sami et al., 2005; Chiba et al., 2000; Armendariz-Picon et al., 2000; Bento et al., 2002; Kamenshchik et al., 2001; Padmanabhan, 2002; Fayaz et al., 2015; Saadat, 2013; Morais et al., 2017) in the scientific literature.

In this study, our primary focus will be on the phenomenon of late cosmic acceleration, a phenomenon that has been observed and supported by numerous observational datasets, including astrophysical observations of Type Ia supernovae (SNe Ia) (Riess et al., 1998; Perlmutter et al., 1999), CMB (Komatsu et al., 2011; Planck Collaboration XVI, 2014), and baryonic acoustic oscillations (BAO) (Eisenstein et al., 2005; Percival et al., 2007). The present model employed to understand late-time cosmic acceleration is known as reconstruction. This approach is essentially the reverse of the process used to identify a suitable cosmological model. Reconstruction methods can be broadly categorized into two types: parametric reconstruction and non-parametric reconstruction (Mukherjee, 2016). Parametric reconstruction relies on the estimation of model parameters using various observational data. It is often referred to as the model-independent approach, as it involves making assumptions about the evolution of the universe based on a specific parametric form. The primary goal of parametric reconstruction is to propose an evolution scenario that accounts for the observed cosmic acceleration and to determine the nature of the matter or exotic components responsible for this acceleration. This method has been extensively discussed in the literature as a means to address various challenges in cosmological investigations. These challenges include the initial singularity problem, the issue of all-time decelerating expansion, the Hubble tension, the horizon problem, and others (Mukherjee, 2016; Banerjee and Das, 2005; Cunha and Lima, 2008; Escamilla-Rivera and Nájera, 2022; Yu-Ting et al., 2010; Gong and Wang, 2006; Mamon and Das, 2016b; El Hanafy and Nashed, 2019; Gong and Wang, 2019).

In our current study, we focus on a generalized dimensionless Hubble parameter model, often referred to as the KMMS (Koussour-Myrzakulov-Myrzakulova-Sofuoğlu) model, which is expressed in terms of redshift (z) as $E^2(z) = \frac{H^2(z)}{H_0^2} = A(z) + \beta(1 + \gamma B(z))$ (Koussour et al., 2023a). This model introduces correction terms associated with DE within the framework of the ΛCDM model. By incorporating these correction terms, we aim to investigate the behavior of the FLRW (Friedmann-Lemaitre-Robertson-Walker) universe within the framework of GR. Several forms of the function $B(z)$ are explored to cover a range of scenarios. These forms include the linear model ($B(z) = z$), the sinusoidal model ($B(z) = \sin(z)$), and the logarithmic model ($B(z) = \log(z + 1)$) (Koussour et al., 2023a). Recently, Koussour et al. (2024) proposed correction terms associated with DE for the Hubble parameter, introducing a correction function $B(z) = \frac{z(1+z)}{1+z^2}$. Each of these forms introduces different characteristics into the model, allowing us to examine a diverse set of cosmic evolution scenarios.

The current paper is organized as follows: Sec. 2 introduces the cosmological model, adopting the parametric form of the dimensionless Hubble parameter. In Sec. 3, we use Bayesian analysis to estimate constraints on the associated free parameters (H_0, Ω_{m0}, γ) using data from recent Cosmic Chronometers (CC) and the $Pantheon^+$ samples. Sec. 4 presents our findings and examines cosmological parameters such as deceleration, jerk, energy density, and EoS parameters to conclude the accelerating behavior of the universe. Finally, Sec. 5 provides a summary and conclusions based on our results.

2. Cosmological model

In the realm of cosmology, the flat Friedmann-Lemaitre-Robertson-Walker (FLRW) metric plays a pivotal role in describing a universe characterized by both isotropy (uniformity in all directions) and homogeneity (uniformity throughout space, where its properties are the same at every point). In the context of a flat FLRW universe, this metric is mathematically expressed by the following equation, as detailed in Ryden (2003):

$$ds^2 = dt^2 - a^2(t)[dr^2 + r^2(d\theta^2 + sin^2\theta d\phi^2)], \tag{1}$$

Here, the symbol $a(t)$ represents the scale factor, which is normalized to unity at the present epoch ($a_0 = 1$). This dimensionless quantity characterizes how the size of the universe evolves with cosmic time t.

Our research is grounded in the theoretical framework of GR. Within the context of the flat FLRW metric, the representation of the energy-momentum tensor for a perfect fluid (a non-viscous fluid) is succinctly expressed as

$$T_{\mu\nu} = (p + \rho) u_\mu u_\nu - p g_{\mu\nu} \tag{2}$$

Here, key physical quantities are involved: u^μ denotes the four-velocity vector, $\rho = \rho_m + \rho_{de}$ combines the total energy density, which comprises contributions from both matter (ρ_m) and DE (ρ_{de}), $p = p_m + p_{de}$ encompasses the total pressure, including contributions from matter pressure ($p_m = 0$) and DE pressure (p_{de}), and $g_{\mu\nu}$ represents the metric tensor, characterizing the geometry of spacetime. It's important to emphasize that the subscript "m" pertains to matter, encompassing both dark matter and baryonic matter, while "de" represents dark energy.

Furthermore, the Einstein field equations of GR elucidate the relationship between the geometry of spacetime and the distribution of matter and energy. In their fundamental form, these equations are represented as $G_{\mu\nu} = \kappa T_{\mu\nu}$, with the simplification $\kappa = 8\pi G = 1$ where $G_{\mu\nu}$ signifies the Einstein tensor, which characterizes the curvature of spacetime. Employing these equations, we can describe the properties of a spatially flat FLRW Universe as follows (Myrzakulov et al., 2023c):

$$3H^2 = \rho_m + \rho_{de}, \tag{3}$$

$$2\dot{H} + 3H^2 = -(p_m + p_{de}) \tag{4}$$

where $H = \frac{\dot{a}}{a}$ represents the Hubble parameter, characterizing the rate of cosmic expansion. In addition, Eqs. (3) and (4) are commonly recognized as the *Friedmann equations*, fundamental tools in the field of cosmology. The first Friedmann equation serves to establish a critical link between the rate of expansion of the Universe and its energy density. It provides crucial insights into how the energy content of the Universe influences the pace at which it is expanding. This equation essentially unveils the intricate interplay between matter, radiation, and DE in shaping the evolution of the cosmos. Conversely, the second Friedmann equation plays a complementary role by elucidating the acceleration of the expansion rate in relation to the pressure within the Universe. It offers a profound understanding of how the presence of pressure, whether positive or negative, exerts a pronounced impact on the dynamics of the cosmic expansion over time. This equation allows cosmologists to explore the effects of different forms of energy and matter on the evolution and fate of our universe, shedding light on its past, present, and future.

Furthermore, the conservation equations for the DE and matter are described as follows:

$$\dot{\rho}_{de} + 3H(\rho_{de} + p_{de}) = 0, \tag{5}$$

$$\dot{\rho}_m + 3H\rho_m = 0. \tag{6}$$

Solving these equations leads to the determination of the energy density for matter:

$$\rho_m(z) = \rho_{m0}(1+z)^3. \tag{7}$$

Here, ρ_{m0} represents an integration constant, which signifies the matter-energy density at the present epoch. The redshift parameter, denoted as z and defined as $z = \frac{1}{a(t)} - 1$, plays a crucial role in understanding the expansion of the universe and the evolution of matter density over time.

Now, among the equations (3)-(6), only three are independent, while we have four unknown parameters: H, ρ_m, ρ_{DE}, and p_{DE}. To successfully solve this system of equations, an additional input is required. It is widely recognized that the parametrization of the Hubble parameter plays a vital role in characterizing the nature of the universe's expansion rate. In general, $H(z)$ can be parametrized in various ways, and one common approach is known as the KMMS models, which express it as (Koussour et al., 2023a):

$$E^2(z) = \frac{H^2(z)}{H_0^2} = A(z) + \beta(1 + \gamma B(z)), \tag{8}$$

where H_0 denotes the present-day expansion rate of the Universe, while β and γ are free parameters. In addition, $A(z)$ and $B(z)$ are functions that rely on the redshift parameter. If $A(z)$ is specified as $A(z) = \Omega_{m0}(1+z)^3$, and the parameters are set to $\beta = \Omega_\Lambda$ and $\gamma = 0$ (or equivalently, $B(z) = 0$), the resulting model is the ΛCDM model,

$$E^2(z) = \Omega_{m0}(1+z)^3 + \Omega_\Lambda, \tag{9}$$

where $\Omega_{m0} = \frac{\rho_{m0}}{3H_0^2}$ represents the current matter density parameter, while $\Omega_\Lambda = \frac{\rho_\Lambda}{3H_0^2}$ signifies the density parameter for the cosmological constant at the present epoch.

In the literature, several cosmological parameterizations have been proposed in linear form to describe various aspects of the universe's evolution. For example, the linear parametrization of the equation of state (EoS) for DE ($\omega(z) = \omega_0 + \omega_1 z$) (Weller and Albrecht, 2002) and the deceleration parameter ($q(z) = q_0 + q_1 z$) (Riess et al., 2004) describe how these parameters evolve with redshift. By introducing a similar linear correction term to the Hubble parameter, we aim to capture comparable time-varying effects in the expansion rate. In this work, we introduce a similar linear correction term to the ΛCDM Hubble parameter to capture comparable time-varying effects in the expansion rate. It is given by

$$A(z) = \Omega_{m0}(1+z)^3\,, \qquad B(z) = z\,. \tag{10}$$

Here, the condition $B(z=0) = 0$ imposes an additional constraint on the model's parameters, reducing their degrees of freedom and resulting in the relation $\Omega_{m0} + \beta = 1$. Consequently, it becomes crucial to compare these models with a range of cosmological data. In the following section, we will integrate various external datasets to ascertain the optimal parameter values for our models, laying the groundwork for subsequent analysis.

3. Cosmological data analysis

In observational cosmology, a crucial aspect is to build precise cosmological models. This requires rigorously constraining model parameters like Ω_{m0}, γ, and the Hubble constant H_0 through the analysis of observational data. In this study, we use a variety of observational datasets, including Cosmic Chronometers (CC) and the latest Pantheon sample ($Pantheon^+$), which consists of observations of SNe Ia.

3.1. Cosmic chronometers (CC) dataset

The CC method is a valuable technique for measuring the Hubble rate. It involves studying the properties of the oldest and most slowly evolving galaxies. These galaxies are selected based on a narrow redshift range, enabling the use of the differential aging method. The Hubble rate H, defined within the FLRW metric, is given by

$$H = -\frac{1}{1+z}\frac{dz}{dt}. \tag{11}$$

This relationship enables us to deduce the universe's expansion rate at different epochs. A major benefit of the CC method is its ability to measure the Hubble parameter $H(z)$ without assuming specific cosmological models. This feature makes the CC method a valuable tool for testing and examining various cosmological models. Notably, R. Jimenez and A. Loeb (2002) proposed a technique to directly obtain Hubble parameter data by calculating the rate of redshift change, dz/dt, at a specific redshift value z. In this study, we assemble a comprehensive dataset consisting of 31 data points from various reputable surveys (Jimenez et al., 2003; Simon et al., 2005; Stern et al., 2010; Moresco et al., 2012; Cong et al., 2014; Moresco, 2015; Moresco et al., 2016; Ratsimbazafy et al., 2017). These data points, derived using the CC method, cover a wide range of redshift values from 0.1 to 2. Among these, 15 data points are correlated and fall within the range $0.179 < z < 1.965$, obtained from measurements in Moresco et al. (2012); Moresco (2015); Moresco et al. (2016). The covariance matrix associated with the CC method can be expressed as

$$Cov_{mn} = Cov^{\mathrm{S}}_{mn} + Cov^{\mathrm{Y}}_{mn} + Cov^{\mathrm{M}}_{mn} + Cov^{\mathrm{SM}}_{mn}. \tag{12}$$

In this context, the superscripts 'S', 'Y', 'M', and 'SM' denote different sources contributing to the covariance matrix: statistical errors, contamination by young components, sensitivity to the chosen model, and variations in stellar metallicity, respectively. The covariance contribution from model-related factors, Cov^{M}_{mn}, can be subdivided into components originating from the star formation history (sfh), initial mass function (imf), stellar library (sl), and the specific stellar population synthesis (sps) model considered: $Cov^{\mathrm{M}}_{mn} = Cov^{\mathrm{sfh}}_{mn} + Cov^{\mathrm{imf}}_{mn} + Cov^{\mathrm{sl}}_{mn} + Cov^{\mathrm{sps}}_{mn}$. In this expression, Cov^{M}_{mn} represents the covariance attributed to general model uncertainties. In addition, Cov^{sfh}_{mn}, Cov^{imf}_{mn}, Cov^{sl}_{mn}, and Cov^{sps}_{mn} indicate contributions stemming from uncertainties related to the star formation history, initial mass function, stellar library, and stellar population synthesis model, respectively.

For conducting an MCMC analysis, it is crucial to calculate the chi-square function for correlated CC measurements, which is defined as

$$\chi^2_{cov}(\vartheta) = (\Delta H) Cov^{-1} (\Delta H)^T, \tag{13}$$

where $\Delta H_k = H_{th}(z_k, \vartheta) - H_{obs}(z_k)$. Now, by incorporating the χ^2 function for the remaining 16 non-correlated CC data points, we obtain

$$\chi^2_{noncov}(\vartheta) = \sum_{k=1}^{16} \left[\frac{(H_{th}(z_k, \vartheta) - H_{obs}(z_k))^2}{\sigma^2_H(z_k)} \right]. \tag{14}$$

In this context, H_{th} represents the theoretical prediction of the Hubble parameter for a specific model with parameters ϑ. H_{obs} denotes the observed values of the Hubble parameter, while σ_H represents the associated error. Therefore, the resulting χ^2 function for the CC dataset is given by

$$\chi^2_{CC} = \chi^2_{cov} + \chi^2_{noncov}. \tag{15}$$

3.2. *Pantheon*$^+$ dataset

The *Pantheon*$^+$ analysis extends the original *Pantheon* study by integrating an enlarged dataset of SNe Ia that includes those with Cepheid distances measured to galaxies. This extensive dataset consists of 1701 light curves from 1550 SNe Ia, covering a redshift range of $0.001 \leq z \leq 2.2613$, sourced from 18 distinct studies (Riess et al., 2022; Brout et al., 2022a,b; Scolnic et al., 2022). Among the 1701 light curves in the dataset, 77 are linked to galaxies containing Cepheids. The *Pantheon*$^+$ compilation represents a substantial improvement over the original *Pantheon* compilation by Scolnic et al. (2018). The enhancements include an expanded sample size, particularly for SNe at redshifts below 0.01. In addition, the *Pantheon*$^+$ compilation addresses systematic uncertainties related to redshifts, intrinsic scatter models, photometric calibration, and peculiar velocities of SNe Ia, leading to notable improvements in data quality. It is important to note that due to specific selection criteria, not all SNe from the original Pantheon compilation are included in the enhanced *Pantheon*$^+$ compilation.

Furthermore, *Pantheon*$^+$ considers the covariance between SNe Ia in its dataset and those located within the Hubble flow. Unlike the original Pantheon sample, which faced challenges in estimating H_0 due to the degeneracy between H_0 and the absolute magnitude M of SNe Ia, the enhanced *Pantheon*$^+$ results overcome this issue. By incorporating both the apparent magnitude m_B and the distance modulus μ^{cd}_k derived from Cepheids associated with SNe in Cepheid host galaxies, the absolute magnitude $M = m_{Bk} - \mu^{cd}_k$ can be independently determined. This separation of the degeneracy between M and H_0 enables an independent assessment of the value of H_0 using the *Pantheon*$^+$ dataset.

To achieve the best fits for the free parameters, it is essential to minimize the χ^2 function, defined as

$$\chi^2_{Pantheon} = \Delta\mu^T (C^{-1}_{Sys+Stat}) \Delta\mu, \tag{16}$$

where $C_{Sys+Stat}$ denotes the covariance matrix of the *Pantheon*$^+$ dataset, which includes both systematic and statistical uncertainties. In addition, $\Delta\mu$ represents the distance residual, defined as

$$\Delta\mu_k = \mu_k - \mu_{th}(z_k). \tag{17}$$

Here, μ_k denotes the distance modulus of the k^{th} SNe Ia. It's calculated as $\mu_k = m_{Bk} - M$, where m_{Bk} is the apparent magnitude of the k^{th} SNe Ia, and M is the fiducial magnitude of a SNe Ia. The theoretical distance modulus μ_{th} is calculated using the expression:

$$\mu_{th}(z, \vartheta) = 5 \log_{10} \left(\frac{d_L(z, \vartheta)}{1 \text{ Mpc}} \right) + 25, \tag{18}$$

where d_L represents the model-derived luminosity distance in megaparsecs (Mpc), defined as

$$d_L(z, \vartheta) = \frac{c(1+z)}{H_0} \int_0^z \frac{dy}{E(y)}. \tag{19}$$

Here, c is the speed of light, and $E(z) = \frac{H(z)}{H_0}$. In addition, the distance residual is denoted by

$$\Delta\bar{\mu} = \begin{cases} \mu_k - \mu^{cd}_k, & \text{if } k \text{ is in Cepheid hosts} \\ \mu_k - \mu_{th}(z_k), & \text{otherwise} \end{cases}. \tag{20}$$

Here, μ^{cd}_k represents the Cepheid host-galaxy distance provided by SH0ES. When calculating the covariance matrix for the Cepheid host-galaxy, it can be merged with the covariance matrix for SNe Ia. The combined covariance matrix, denoted as $C^{SNe}_{Sys+Stat} + C^{cd}_{Sys+Stat}$, includes both statistical and systematic uncertainties from the *Pantheon*$^+$ dataset. Therefore, the χ^2 function for the combined covariance matrix used to constrain cosmological models in the analysis is expressed as

$$\chi^2_{Pantheon^+} = \Delta\bar{\mu} (C^{Pantheon}_{Sys+Stat} + C^{cd}_{Sys+Stat})^{-1} \Delta\bar{\mu}^T. \tag{21}$$

3.3. *CC+ Pantheon*$^+$ dataset

To perform a joint analysis of the CC and *Pantheon*$^+$ datasets, we define the χ^2_{joint} function as

$$\chi^2_{joint} = \chi^2_{CC} + \chi^2_{Pantheon^+}. \tag{22}$$

In this study, we employ the standard Bayesian technique to estimate the values of the model's free parameters (Hobson et al., 2009). The prior distribution used for these parameters is detailed in Table 1. The range of $[-10, 10]$ for γ covers a broad spectrum of potential values, as γ is associated with the linear correction term in the Hubble parameter and can be positive or negative. This range was selected to ensure that various scenarios are considered, allowing the data to determine the most probable value within this range. The prior range of $[0, 1]$ for Ω_{m0} is standard in cosmology, reflecting the plausible range of the matter density parameter in a flat universe. Values outside this range suggest a non-flat universe, which is less supported by observational and theoretical findings.

By sampling the probability functions derived from the combined data of CC and *Pantheon*$^+$, we employed a robust Markov Chain Monte Carlo (MCMC) method implemented in Python using the *emcee* (Mackey et al., 2013) software. In our MCMC analysis, we utilized 100 walkers and conducted 1000 steps to explore the parameter space and estimate the likelihood distributions. This approach allowed us to identify the region in the parameter space with the highest probability of containing the values of the free parameters of the model. The results of this analysis are depicted in Fig. 1, where the contours represent the $1-\sigma$ and $2-\sigma$ confidence levels (corresponding to 68% and 95% confidence levels, respectively). In Table 1, we present the values of the free parameters of the model within a 95% confidence interval. We find that $\Omega_{m0} = 0.249^{+0.027}_{-0.026}$. In addition, the constraints obtained for the model parameter γ indicate that it takes a small negative value, specifically $\gamma = -0.17^{+0.35}_{-0.35}$, representing a slight deviation from ΛCDM. Moreover, the Hubble constant for the model is determined to be $H_0 = 72.4^{+2.5}_{-2.5}$ km/s/Mpc. Notably, this value for H_0 is consistent with the results obtained from the SH0ES project (Riess et al., 2019), where $H_0 = 74.03 \pm 1.42$ km/s/Mpc (at the 1σ confidence level), indicating tension with the Planck results ($H_0 = 67.4 \pm 0.5$ km/s/Mpc) (Planck Collaboration, 2020).

3.4. Information criteria

Here, we will examine different statistical criteria and methods for selecting models. Specifically, we will employ the Akaike information criterion (AIC) (Akaike, 1974) and the Bayesian information criterion (BIC) (Schwarz, 1978) to evaluate the predictive performance of various models using datasets. The AIC tackles the issue of model adequacy by acting as an estimator of Kullback-Leibler information, showing asymptotically unbiased properties. Defined under the assumption of Gaussian

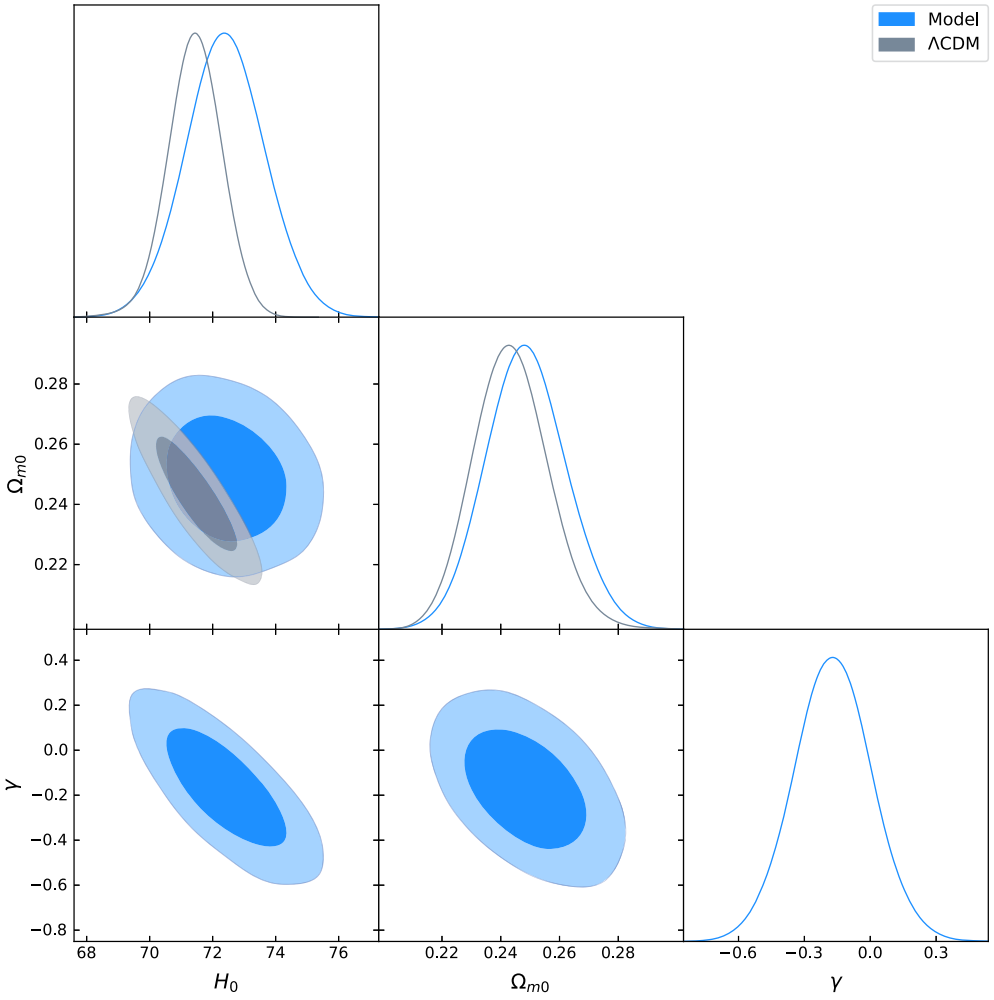

Fig. 1. The model parameters' constraints derived from the combined $H(z) + Pantheon$ dataset are depicted by contours representing the 68% and 95% confidence levels (C.L.).

Table 1
Selected prior distributions and best-fit values for the free parameters obtained from the combined $H(z) + Pantheon$ dataset.

Parameter	Prior interval	Model	ΛCDM
H_0 (km/s/Mpc)	$[60, 80]$	$72.4^{+2.5}_{-2.5}$	$71.4^{+1.7}_{-1.7}$
Ω_{m0}	$[0, 1]$	$0.249^{+0.027}_{-0.026}$	$0.244^{+0.026}_{-0.024}$
γ	$[-10, 10]$	$-0.17^{+0.35}_{-0.35}$	–
χ^2_{min}	–	1714.58	1712.99
AIC	–	1720.58	1716.99
ΔAIC	–	3.59	0
BIC	–	1724.30	1719.45
ΔBIC	–	4.85	0

errors, the AIC estimator is given by (Spiegelhalter et al., 2002; Anderson, 2002),

$$AIC = -2\ln(\mathcal{L}_{max}) + 2k + \frac{2k(k+1)}{N_{tot} - k - 1}. \tag{23}$$

Here, k represents the number of parameters in the model, $\mathcal{L}_{max}$ is the maximum likelihood value of the datasets being analyzed, and N_{tot} denotes the total number of data points. For large datasets, the formula simplifies to $AIC \equiv -2\ln(\mathcal{L}_{max}) + 2k$ (Burnham and Anderson, 2004), which is a modified AIC criterion that is universally applicable. Further, the BIC, serving as a Bayesian evidence estimator (Anderson, 2002; Burnham and Anderson, 2004; Liddle, 2007), is formulated as

$$BIC = -2\ln(\mathcal{L}_{max}) + k\log(N_{tot}). \tag{24}$$

Here, $\chi^2_{min} = -2\ln(\mathcal{L}_{max})$. To rank a series of competing models based on their fit to observational data, we apply the aforementioned criteria. Our focus is particularly on the relative difference in Information Criterion (IC) values among the considered models. This difference denoted as $\Delta IC_{model} = IC_{model} - IC_{min}$, compares each model's IC value to the minimum IC value among the competing models. According to Jeffreys' scale (Kass and Raftery, 1995), if the difference in IC values, ΔIC, is less than or equal to 2, the model is statistically in agreement with the most favored model by the data. A difference in IC values falling between 2 and 6 suggests a moderate tension between the two models, whereas a difference of 10 or more indicates a significant tension. To conduct these tests, we use the ΛCDM model as a reference and compare it with our model. We then constrain the parameters H_0 and Ω_{m0} of the ΛCDM model using the aforementioned datasets, and the outcomes are shown in Table 1. These results are employed in further model selection analyses. The results of the model selection analysis are also presented in Table 1. From these findings, we observe that $2 < \Delta IC < 6$ for each comparison, indicating a moderate tension between the two models.

4. Findings and cosmological parameters

In this section, we will delve into the behavior of cosmological parameters that describe the evolutionary phases of the universe. These

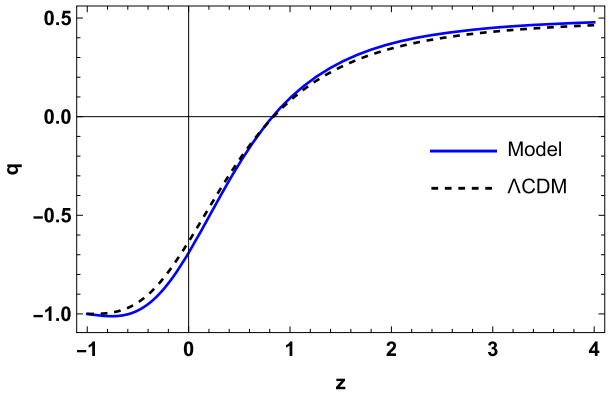

Fig. 2. Plot of the deceleration parameter q as a function of the redshift z.

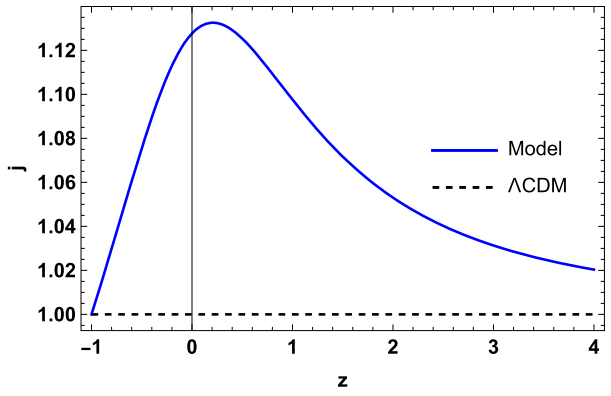

Fig. 3. Plot of the jerk parameter q as a function of the redshift z.

parameters correspond to the values extracted from the model parameters generated by the *emcee* software.

Firstly, the sign of the deceleration parameter (q), expressed as $q = -1 - \frac{\dot{H}}{H^2}$, provides key insights into the nature of the universe's expansion. When $q > 0$, the model indicates decelerating expansion, suggesting that the gravitational pull of matter is slowing down the universe's rate of expansion. If $q = 0$, the expansion is at a constant rate, while for $-1 < q < 0$, the model indicates accelerating expansion, indicating that some form of repulsive force, such as DE, is driving the expansion. For $q = -1$, the universe exhibits exponential expansion, also known as de Sitter expansion, characterized by an accelerating expansion driven by a cosmological constant. For $q < -1$, the expansion is super-exponential, indicating a rapid acceleration beyond the de Sitter expansion rate. In our model, the deceleration parameter is given by the following equation:

$$q = -1 + \frac{(1+z)\left(-\gamma\Omega_{m0} + \gamma + 3\Omega_{m0}(1+z)^2\right)}{2(\Omega_{m0}z(-\gamma + z(3+z)+3) + \gamma z + 1)}. \tag{25}$$

From Eq. (25), it becomes evident that our models ultimately display a phase of super-exponential expansion ($q < -1$ at $z < 0$), and as time progresses, they approach a phase of exponential expansion ($q = -1$ at $z \to -1$). This behavior signifies an intriguing transition in the universe's evolution, where the expansion rate undergoes a significant change over time. In Fig. 2, we depict the plot of the deceleration parameter versus redshift (z). This plot serves as a visual representation of the evolution of the universe's expansion dynamics. One notable feature revealed by the plot is a distinctive transition from a phase of decelerating expansion to a phase of accelerating expansion at a redshift value $z_t = 0.83^{+0.11}_{-0.10}$ with the present value $q_0 = -0.69^{+0.17}_{-0.17}$, which are close to ΛCDM model as shown in the same figure (Mamon and Das, 2016b; El Hanafy and Nashed, 2019; Gong and Wang, 2019). This transition, known as a signature flip, marks a pivotal shift in the dominant forces governing the universe's expansion, highlighting the complex interplay between gravitational attraction and the repulsive effects of DE.

The jerk parameter is another crucial dimensionless parameter that provides valuable insights into the dynamics of the universe's expansion. Unlike the deceleration parameter, which measures the rate of change of the expansion rate, the jerk parameter characterizes the rate of change of the acceleration of the universe's expansion. Mathematically, the jerk parameter (j) is defined as the third derivative of the cosmic scale factor (a) with respect to cosmic time (t), normalized by the cube of the Hubble parameter (H) (Sahni et al., 2003; Visser, 2004):

$$j(z) = \frac{\dddot{a}}{aH^3} = q(2q+1) + (1+z)\frac{dq}{dz}. \tag{26}$$

For our model, the expression for the jerk parameter $j(z)$ is given by

$$j(z) = \frac{\gamma(\Omega_{m0} - 1) + \Omega_{m0}z(z(3+z)+3) + 1}{\Omega_{m0}z(-\gamma + z(3+z)+3) + \gamma z + 1}. \tag{27}$$

However, the jerk parameter provides an indication of how the model's behavior deviates from the predictions of the flat ΛCDM model, where $j = 1$. In the best-fit model, the value of the jerk parameter is found to deviate from this standard value, reflecting a departure from the behavior expected in a simple cosmological constant scenario. In the context of our model (refer to Fig. 3), the present value of j is greater than 1 ($j_0 = 1.13^{+0.26}_{-0.26}$) for the datasets considered, and it converges to the standard ΛCDM value of $j = 1$ in the near future (Mamon and Bamba, 2018). This observation indicates that, within the framework of our model, the current state of the universe exhibits a higher rate of change in acceleration compared to what is predicted by the flat ΛCDM model.

Consequently, based on the model under consideration, where both $j_0 > 0$ and $q_0 < 0$, it becomes apparent that the dynamic DE model being studied presents the most probable explanation for the observed acceleration of the universe at present times.

Now, let's delve into the physical parameters of the model, specifically focusing on the dimensionless energy density parameters associated with matter and DE. These parameters play a crucial role in describing the composition of the universe and its evolution over time. Mathematically, they are expressed as

$$\Omega_m = \frac{\rho_m}{3H^2}, \qquad \Omega_{de} = \frac{\rho_{de}}{3H^2}. \tag{28}$$

If the dimensionless matter density parameter (Ω_m) is close to 1, it signifies that matter dominates the universe's energy density, resulting in a decelerating cosmic expansion. This scenario aligns with the behavior expected in a universe primarily composed of matter, where gravitational attraction slows down the expansion over time. On the other hand, in the presence of a cosmological constant (Λ) associated with DE, the dimensionless DE density parameter (Ω_{de}) remains approximately constant over cosmic time. In this context, DE gradually becomes the dominant component of the universe's energy density, eventually driving the universe into a phase of accelerated expansion. This behavior is consistent with the observed acceleration of the universe's expansion in the late stages of its evolution.

By using Eqs. (8) and (28), we obtain

$$\Omega_m(z) = \frac{\Omega_{m0}(1+z)^3}{\Omega_{m0}z(-\gamma + z(3+z)+3) + \gamma z + 1}, \tag{29}$$

$$\Omega_{de}(z) = 1 - \Omega_m(z). \tag{30}$$

In Fig. 4, we present the evolution of the dark sector within the context of the scenario under consideration. The graph illustrates the evolving behavior of the dimensionless energy density parameters associated with matter (Ω_m) and DE ($\Omega_{de} = 1 - \Omega_m$). Notably, the present value of Ω_{m0} is found to be $\Omega_{m0} = 0.249^{+0.027}_{-0.026}$, which is consistent with the findings from Planck observations (Planck Collaboration, 2020), based on the combined CC+ *Pantheon*$^+$ data. The graph reveals the familiar thermal history of the universe, characterized by distinct epochs

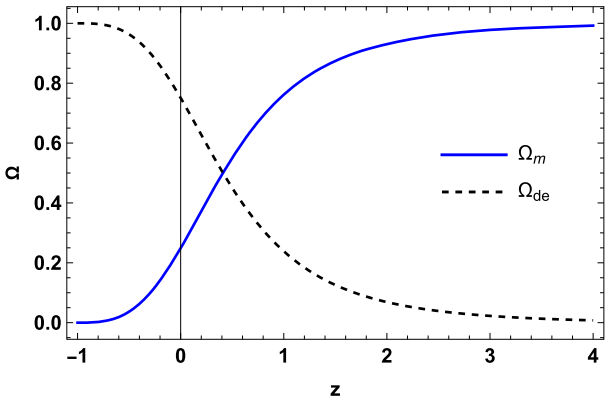

Fig. 4. Plot of the dimensionless energy density as a function of the redshift z.

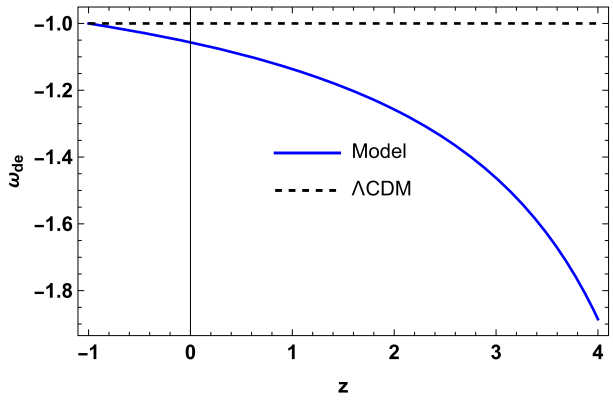

Fig. 5. Plot of the EoS parameter ω_{de} as a function of the redshift z.

dominated by matter and DE. In the future, the universe is shown to asymptotically approach a dark-energy-dominated de Sitter phase. This behavior is indicative of the universe's transition towards a phase of accelerated expansion driven by DE, consistent with the current understanding of cosmic evolution.

In addition, we consider the EoS parameter that describes the relationship between the DE density and its pressure:

$$\omega_{de} = \frac{p_{de}}{\rho_{de}} = -\frac{2\dot{H} + 3H^2}{3H^2 - \rho_m} \tag{31}$$

Using (8) and (31), we have

$$\omega_{de}(z) = \frac{\gamma - 2\gamma z - 3}{3\gamma z + 3}. \tag{32}$$

The EoS parameter ω_{de} is instrumental in characterizing the behavior of the universe's expansion, specifically in distinguishing between decelerating and accelerating phases. This parameter classifies the accelerating universe into three distinct states: the quintessence era ($-1 < \omega_{de} < -\frac{1}{3}$), the phantom era ($\omega_{de} < -1$), and the cosmological constant era ($\omega_{de} = -1$) (Koussour et al., 2023b,c; Myrzakulov et al., 2023a,b). In Fig. 5, we illustrate the evolutionary trajectory of the EoS parameter. The graph depicts its behavior over cosmic time, highlighting its transition between different phases. At high redshifts, the EoS parameter tends to lie within the phantom regime ($\omega_{de} < -1$), indicating a phase where DE exhibits particularly strong negative pressure. However, as time progresses, it approaches the cosmological constant value of -1. Furthermore, we observe that the EoS reaches a singularity, or pole, when the parameter $\gamma < 0$. Consequently, the EoS for DE approaches infinity under these conditions. This behavior of DE indicates an exotic and extreme nature, potentially causing significant changes in the universe's large-scale structure and expansion dynamics (Özülker, 2022). Our analysis yields a current value of the EoS parameter, ω_{de0}, to be within the range $\omega_{de0} = -1.06 \pm 0.12$. This result is consistent with several previous studies (Mukherjee, 2016; Gong and Wang, 2019; Novosyadlyj and Sergijenko, 2012; Kumar and Xu, 2014), which also suggest an accelerating phase for the universe. This alignment with existing research further supports the notion of an accelerating universe driven by DE.

5. Conclusions

In conclusion, this study has delved into the cosmological evolution of the universe, driven by the intriguing characteristics of the model-independent approach, particularly the KMMS models (Koussour et al., 2023a). Our focus has been on the scenario involving the linear correction, i.e. $B(z) = z$, aiming to explore its implications and potential insights into the dynamics of cosmic evolution. Through our analysis, we focused on recent Cosmic Chronometers (CC) and the *Pantheon*$^+$ samples. Using a Markov chain Monte Carlo analysis of the model, we were able to determine the best-fit values of the model parameters (see Table 1 and Fig. 1).

In addition, our analysis has provided insights into various key parameters that describe the dynamics of cosmic expansion, shedding light on the universe's behavior over time. Regarding the deceleration parameter (see Fig. 2), our models exhibit a phase of super-exponential expansion ($q < -1$ at $z < 0$), transitioning towards an exponential expansion phase ($q = -1$ at $z \to -1$). This transition signifies a significant change in the universe's expansion dynamics, with a distinctive shift from decelerating to accelerating expansion at a redshift value $z_t = 0.83^{+0.11}_{-0.10}$ and a present value $q_0 = -0.69^{+0.17}_{-0.17}$. Concerning the jerk parameter (see Fig. 3), observational data suggests that the current value exceeds 1 ($j_0 = 1.13^{+0.26}_{-0.26}$), indicating a higher rate of change in acceleration compared to the predictions of the flat ΛCDM model. This observation provides further evidence for the unique dynamics described by our model. The analysis of the energy density parameter reveals a present value of $\Omega_{m0} = 0.249^{+0.027}_{-0.026}$, consistent with Planck observations. The evolution of the dark sector, as illustrated in Fig. 4, follows the expected thermal history of the universe, with distinct epochs dominated by matter and DE. In the future, the universe is projected to transition towards a dark-energy-dominated de Sitter phase, indicative of an accelerated expansion driven by DE.

Finally, the examination of the EoS parameter, as depicted in Fig. 5, indicates its gradual approach towards the cosmological constant value of $\omega_{de} = -1$ over cosmic time. Our analysis yields a current value of $\omega_{de0} = -1.06 \pm 0.12$, aligning with the phantom phase. The cosmological dynamics of the universe with a phantom energy component offer numerous intriguing features (Caldwell et al., 2003). Detailed analyses of the Lagrangians describing phantom energy reveal that, in some cases, the universe with phantom energy culminates in a 'big rip', while in others, it asymptotically approaches de Sitter expansion (McInnes, 2002). Furthermore, the uncertainties associated with the value of ω_{de} vary according to the deviations from the ΛCDM model. Another compelling aspect is the Hubble constant (H_0) tension. Several attempts to resolve this tension through new physics have relied on extended cosmological models. Refs. Vagnozzi (2020); Di Valentino et al. (2016) suggest that a phantom-like component with an effective EoS $\omega_{de0} = -1.29$ can resolve the current tension between the Planck dataset and other priors within an extended ΛCDM scenario. Notably, our obtained model lies in the Phantom phase with the EoS $\omega_{de0} = -1.13$. Therefore, our model may have the potential to alleviate some of the tension at the present point.

The differences observed in the values and behaviors of the equation of state parameter from the ΛCDM model indicate the potential existence of a new DE alternative. The KMMS model emerges as a promising candidate for explaining the accelerated expansion of the universe and addressing new cosmic findings. Its ability to capture distinct features of cosmic evolution suggests that it may offer valuable insights into the nature of DE and the dynamics of the universe on a larger scale.

This highlights the importance of considering alternative models like the KMMS model in our quest to unravel the mysteries of the cosmos.

CRediT authorship contribution statement

Yerlan Myrzakulov: Writing – review & editing, Writing – original draft, Formal analysis, Data curation, Conceptualization. **M. Koussour:** Writing – review & editing, Writing – original draft, Formal analysis, Data curation, Conceptualization. **M. Karimov:** Investigation, Methodology, Writing – original draft. **J. Rayimbaev:** Writing – review & editing, Writing – original draft, Formal analysis, Data curation, Conceptualization.

Declaration of competing interest

The authors declare that they have no known competing financial interests or personal relationships that could have appeared to influence the work reported in this paper.

Data availability

All data used in this study are cited in the references and were obtained from publicly available sources.

Acknowledgment

This research was funded by the Science Committee of the Ministry of Science and Higher Education of the Republic of Kazakhstan (Grant No. AP22682760).

References

Abdalla, E., et al., 2022. JHEAp 34, 49–211.
Addazi, A., et al., 2022. Prog. Part. Nucl. Phys. 125, 103948.
Akaike, H., 1974. IEEE Trans. Autom. Control 19, 716.
Anderson, K., 2002. Model Selection and Multimodel Inference: A Practical Information-Theoretic Approach, 2nd ed. Springer, New York.
Armendariz-Picon, C., et al., 2000. Phys. Rev. Lett. 85, 4438.
Banerjee, N., Das, S., 2005. Gen. Relativ. Gravit. 37, 1695.
Bento, M.C., et al., 2002. Phys. Rev. D 66, 043507.
Brout, D., et al., 2022a. Astrophys. J. 938, 110.
Brout, D., et al., 2022b. Astrophys. J. 938, 111.
Buchdahl, H.A., 1970. Mon. Not. R. Astron. Soc. 150, 1.
Burnham, K.P., Anderson, D.R., 2004. Sociol. Methods Res. 33, 261.
Caldwell, R.R., Kamionkowski, M., Weinberg, N.N., 2003. Phys. Rev. Lett. 91, 071301.
Capozziello, S., et al., 2011. Phys. Rev. D 84, 043527.
Capozziello, S., Nojiri, S., Odintsov, S.D., 2018. Phys. Lett. B 781, 99–106.
Chiba, T., et al., 2000. Phys. Rev. D 62, 023511.
Cong, Z., et al., 2014. Res. Astron. Astrophys. 14, 1221.
Cunha, J.V., Lima, J.A.S., 2008. Mon. Not. R. Astron. Soc. 390, 210.
Di Valentino, E., et al., 2016. Phys. Lett. B 761, 242–246.
Eisenstein, D.J., et al., 2005. Astrophys. J. 633, 560–574.
El Hanafy, W., Nashed, G.G.L., 2019. Phys. Rev. D 100, 083535.
Escamilla-Rivera, C., Nájera, A., 2022. J. Cosmol. Astropart. Phys. 03, 060.
Fayaz, V., et al., 2015. Eur. Phys. J. Plus 130, 1–12.
Freedman, W.L., 2017. Nat. Astron. 1, 0121.
Gong, Y., Wang, A., 2006. Phys. Rev. D 73, 083506.
Gong, Y., Wang, A., 2019. Phys. Rev. D 75, 043520.
Hobson, M.P., Jaffe, A.H., Liddle, A.R., Mukherjee, P., Parkison, D. (Eds.), 2009. Bayesian Methods in Cosmology. Cambridge 197 University Press, Cambridge, England.
Jimenez, J.B., et al., 2018. Phys. Rev. D 98, 044048.
Jimenez, J.B., et al., 2020. Phys. Rev. D 101, 103507.
Jimenez, R., Loeb, A., 2002. Astrophys. J. 573, 340549.
Jimenez, R., et al., 2003. Astrophys. J. 593, 622.
Kamenshchik, A.Y., et al., 2001. Phys. Lett. B 511, 265.
Kass, R.E., Raftery, A.E., 1995. J. Am. Stat. Assoc. 90, 773.
Kleinert, H., Schmidt, H.J., 2002. Gen. Relativ. Gravit. 34, 1295.
Komatsu, E., et al., 2011. Astrophys. J. Suppl. Ser. 192, 18.
Koussour, M., et al., 2023a. Results Phys. 55, 107166.
Koussour, M., et al., 2023b. Phys. Dark Universe 42, 101339.
Koussour, M., et al., 2023c. Eur. Phys. J. C 83, 1–14.
Koussour, M., et al., 2024. J. High Energy Astrophys. 42, 96–103.
Kumar, S., Xu, Lixin, 2014. Phys. Lett. B 737, 244.
Liddle, A.R., 2007. Mon. Not. R. Astron. Soc. 377, L74.
Lin, W., Mack, K.J., Hou, L., 2020. Astrophys. J. Lett. 904, L22.
Liu, Di, Reboucas, M.J., 2012. Phys. Rev. D 86, 083515.
Lusso, E., et al., 2019. Astron. Astrophys. 628, L4.
Mackey, D.F., et al., 2013. Publ. Astron. Soc. Pac. 125, 306.
Mamon, A.A., Das, S.A., 2016b. Int. J. Mod. Phys. D 25, 1650032.
Mamon, A. Al, Bamba, K., 2018. Eur. Phys. J. C 78, 862.
Martin, J., 2012. C. R. Phys. 13, 566–665.
McInnes, B., 2002. J. High Energy Phys. 0208, 029.
Morais, J., et al., 2017. Phys. Dark Universe 15, 7–30.
Moresco, M., 2015. Mon. Not. R. Astron. Soc. Lett. 450, L16.
Moresco, M., et al., 2012. J. Cosmol. Astropart. Phys. 08, 006.
Moresco, M., et al., 2016. J. Cosmol. Astropart. Phys. 05, 014.
Mukherjee, A., 2016. Mon. Not. R. Astron. Soc. 460, 273–282.
Myrzakulov, N., et al., 2023a. Eur. Phys. J. Plus 138, 852.
Myrzakulov, N., et al., 2023b. Chin. Phys. C 47, 115107.
Myrzakulov, N., Koussour, M., Gogoi, D.J., 2023c. Eur. Phys. J. C 83, 594.
Novosyadlyj, B., Sergijenko, O., 2012. Phys. Rev. D 86, 083008.
Odintsov, S.D., Oikonomou, V.K., 2017. Phys. Rev. D 96 (10), 104049.
Özülker, E., 2022. Phys. Rev. D 106, 063509.
Padmanabhan, T., 2002. Phys. Rev. D 66, 021301.
Percival, W.J., et al., 2007. Mon. Not. R. Astron. Soc. Lett. 381, 1053.
Perivolaropoulos, L., Skara, F., 2022. New Astron. Rev. 95, 101659.
Perlmutter, S., et al., 1999. Astrophys. J. 517, 565.
Planck Collaboration XVI, 2014. Astron. Astrophys. 571, A16.
Planck Collaboration, 2020. Astron. Astrophys. 641, A6.
Ratra, B., Peebles, P.J.E., 1998. Phys. Rev. D 37, 3406.
Ratsimbazafy, A.L., et al., 2017. Mon. Not. R. Astron. Soc. 467, 3239.
Riess, A.G., et al., 1998. Astron. J. 116, 1009.
Riess, A.G., et al., 2004. Astrophys. J. 607, 665.
Riess, A.G., et al., 2019. Astrophys. J. 876, 85.
Riess, A.G., et al., 2022. Astrophys. J. Lett. 934, L7.
Ryden, B., 2003. Introduction to Cosmology. Addison Wesley, San Francisco, CA, USA.
Saadat, H., 2013. Int. J. Theor. Phys. 52, 1027–1032.
Sahni, V., et al., 2003. JETP Lett. 77, 201–206.
Sami, M., Toporensky, A., 2004. Mod. Phys. Lett. A 19, 1509.
Sami, M., et al., 2005. Phys. Lett. B 619, 193.
Schwarz, G., 1978. Ann. Stat. 6, 461.
Scolnic, D., et al., 2022. Astrophys. J. 938, 113.
Scolnic, D.M., et al., 2018. Astrophys. J. 859, 101.
Simon, J., Verde, L., Jimenez, R., 2005. Phys. Rev. D 71, 123001.
Spiegelhalter, D.J., Best, N.G., Carlin, B.P., van der Linde, A., 2002. J. R. Stat. Soc. 64, 583.
Steinhardt, P.J., et al., 1999. Phys. Rev. Lett. 59, 123504.
Stern, D., et al., 2010. J. Cosmol. Astropart. Phys. 02, 008.
Vagnozzi, S., 2020. Phys. Rev. D 102, 023518.
Visser, M., 2004. Gen. Relativ. Gravit. 37, 1541–1548.
Weinberg, S., 1989. Rev. Mod. Phys. 61, 1.
Weller, J., Albrecht, A., 2002. Phys. Rev. D 65, 103512.
Yu-Ting, W., et al., 2010. Chin. Phys. B 19, 019801.